

DOI:10.1002/ejic.201201387

Triptycene-Based, Carboxylate-Bridged Biomimetic Diiron(II) Complexes

Yang Li,^[a] Chan Myae Myae Soe,^[a] Justin J. Wilson,^[a]
Suan Lian Tuang,^[a] Ulf-Peter Apfel,^[a] and Stephen J. Lippard*^[a]

Keywords: Enzyme models / Iron / Oxygenases / Ligand design / Triptycene

A triptycene-based bis(benzimidazole) ester ligand, **L3**, was designed to enhance the electron-donating ability of the heterocyclic nitrogen atoms relative to those of the first-generation bis(benzoxazole) analogs, **L1** and **L2**. A convergent synthesis of **L3** was designed and executed. Three-component titration experiments using UV/Vis spectroscopy revealed that the desired diiron(II) complex could be obtained with a 1:2:1 ratio of **L3**/Fe(OTf)₂(MeCN)₂/external carboxylate reactants. X-ray crystallographic studies of two diiron complexes derived in this manner from **L3** revealed their formulas to be [Fe₂L3(μ-OH)(μ-O₂CR)(OTf)₂], where R = 2,6-bis(*p*-tolyl)-

phenyl (**7**) or triphenylmethyl (**8**). The structures are similar to that of a diiron complex derived from **L1**, [Fe₂L1(μ-OH)(μ-O₂CAr^{Tol})(OTf)₂] (**9**), a notable difference being that, in **7** and **8**, the geometry at iron more closely resembles square-pyramidal than trigonal-bipyramidal. Mössbauer spectroscopic analyses of **7** and **8** indicate the presence of high-spin diiron(II) cores. These results demonstrate the importance of substituting benzimidazole for benzoxazole for assembling biomimetic diiron complexes with *syn* disposition of two *N*-donor ligands, as found in O₂-activating carboxylate-bridged diiron centers in biological systems.

Introduction

Bacterial multicomponent monooxygenases (BMMs), including soluble methane monooxygenase (sMMO),^[1] toluene monooxygenase (ToMO),^[2,3] and phenol hydroxylase (PH),^[4] belong to a unique family of carboxylate-bridged diiron enzymes.^[5–8] The diiron active sites of BMMs have an oxygen-rich coordination environment composed of terminal and bridging carboxylates, water and/or hydroxides, and two imidazole donors that bind in a *syn* fashion with respect to the diiron vector. Even though the active sites of members of the BMM family are very similar in structure, each enzyme catalyzes the oxidation or epoxidation of a specific set of hydrocarbon substrates.

The coordination environment of the diiron core of soluble methane monooxygenase hydroxylase (sMMOH) is provided by a highly preorganized set of amino acid residues. The proper orientation of these coordinating residues is maintained by the predefined conformation of the folded protein. The empty active site of the apo-form of sMMOH, for example, is structurally analogous to that containing the coordinated diiron unit.^[9] This high degree of preorganization is a feature common to many enzymes.^[10] In addition

to serving as a structural scaffold, the active site cavity also provides a hydrophobic environment where catalytic intermediates can avoid being prematurely deactivated by adventitious reactants.

The synthesis of faithful small-molecule models of the active sites of diiron enzymes is a significant challenge in bioinorganic chemistry.^[11–17] In addition to providing a platform for studying the mechanisms of natural systems, biomimetic models may also function as catalysts to perform similar chemical transformations. Over the past three decades, many different ligands have been employed to mimic the diiron cores of BMMs. Among them, ligands based on tris(2-pyridylmethyl)amine (TPA) and sterically encumbering 2,6-diarylbenzoate ligands have been extensively investigated (Figure 1).^[13,14,18,19] Although much insight has been gained from studying these systems, the model compounds generally fall short of accurately replicating both the structural and electronic properties of the enzyme active site, not to mention their functions. TPA-based diiron complexes can generate intermediates close to those observed in BMMs upon reaction with dioxygen. These intermediates usually exhibit poor reactivity with hydrocarbons, which may be due to the fact that they have a low-spin rather than a high-spin electronic configuration^[20–22] as a result of their nitrogen- rather than oxygen-rich coordination environments.^[23–25] High-spin diiron complexes of this ligand class are more reactive.^[26–30] Sterically encumbering 2,6-diarylbenzoate ligands form diiron complexes that closely mimic the oxygen-rich coordination sphere found in the active sites of BMMs.^[31–34] The use of

[a] Department of Chemistry, Massachusetts Institute of Technology, Cambridge, MA 02139, USA
Fax: +1-617-258-8150
E-mail: lippard@mit.edu
Homepage: <http://web.mit.edu/lippardlab/>

Supporting information for this article is available on the WWW under <http://dx.doi.org/10.1002/ejic.201201387>.

dendrimer-appended carboxylates allowed preparation of complexes having a hydrophobic sheath, similar to the environment surrounding the diiron active sites of the BMMs.^[35] Attempts to model the *syn* disposition of the two histidine ligands in this system, however, led only to the formation of complexes with nitrogen donors in the *anti* disposition. Thus, although certain structures and reactivities of the BMM active site can be modeled, no small molecule yet exists that can successfully mimic both features.

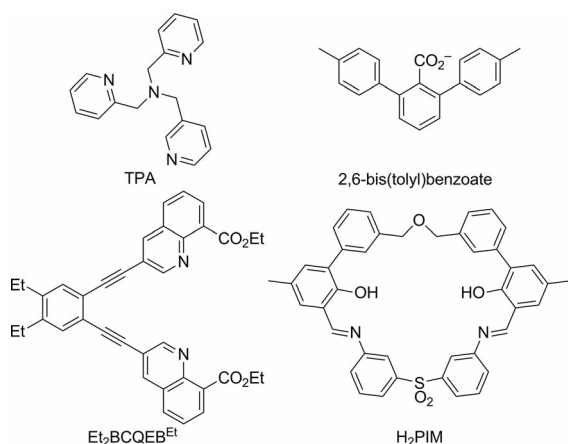


Figure 1. Ligands employed in diiron modeling.

Our group has recently focused on constructing faithful structural models by using tailor-made dinucleating ligands. A particularly challenging aspect is to model the *syn* disposition of the two histidine ligands. This orientation of nitrogen donors may be crucial for the oxidation of methane by intermediate **Q** of sMMOH.^[22] We have prepared and reported several ligands with the goal of modeling this structural feature.^[14,16,17,36] 1,2-Diethynylbenzene-based scaffolds were effectively employed for this purpose.^[37–41] The low-energy barrier to rotation about the alkyne C–C bond, however, led to the formation of undesired metallopolymers and bis(ligand)iron complexes.^[38,42] To circumvent this problem, we recently introduced a *syn* *N*-donor macrocyclic ligand, H₂PIM,^[43] which afforded a diiron complex with remarkable structural similarity to the active site of sMMOH.

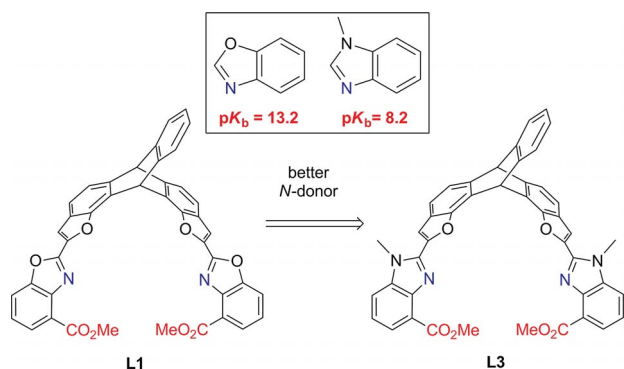


Figure 2. More basic benzimidazole ligand.

Here, we describe an advanced design of highly preorganized ligands for the synthesis of biomimetic models of the diiron active site of sMMOH (Figure 2). Continuing along lines reported previously,^[36] we present the synthesis of a new ligand with a triptycene backbone, **L3**. This molecule differs from previously reported triptycene **L1**^[36] by replacement of the benzoxazole arms with more nucleophilic benzimidazole donors. The synthesis and structures of two carboxylate-bridged diiron(II) complexes of **L3** are reported, and the results are compared to those for the **L1** analogue.

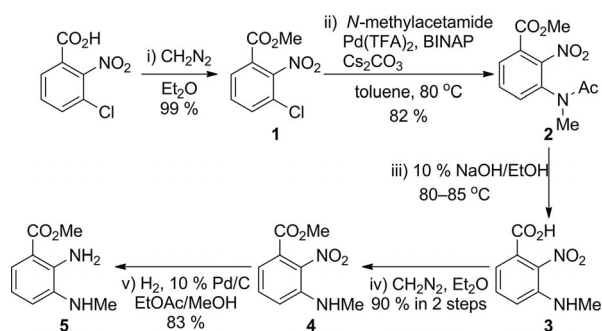
Results and Discussion

Ligand Design and Synthesis

We previously reported a unique dinucleating ligand having two benzoxazole *N,O*-donor arms linked through a rigid triptycene backbone (Figure 2, **L1**).^[36] With this ligand, we were able to crystallize and obtain structural data for the diiron complex, [Fe₂L1(μ-OH)(μ-O₂CAr^{Tol})(OTf)₂], where each iron atom is coordinated by the nitrogen atom of the benzoxazole group and an oxygen atom from the ester. Because the active site of sMMOH utilizes carboxylate rather than ester groups, the analogous ligand, H₂L^{Ph4}, which bears sterically protected bis(benzoxazole) diacid ligands, was synthesized.^[44] The coordination of H₂L^{Ph4} to iron in the presence of an external carboxylate afforded the unanticipated triiron complex, [NaFe₃(L^{Ph4})₂(μ₃-O)(μ-O₂CCPh₃)₂(H₂O)₃](OTf)₂, having a “basic iron acetate” core.^[44] A noteworthy feature of the [NaFe₃(L^{Ph4})₂(μ₃-O)(μ-O₂CCPh₃)₂(H₂O)₃](OTf)₂ structure is the lack of iron coordination at the nitrogen atoms of the benzoxazole arms. We hypothesized that these nitrogen atoms do not bind to the iron centers because of the low basicity of the benzoxazole moiety (p*K*_b = 13.2). Much more basic nitrogen donors are provided by the bis(benzimidazole) ligand, **L3** (Figure 2). The p*K*_b of benzimidazole is 8.2, which is five orders of magnitude more basic than that of benzoxazole; this increase in basicity was expected to enhance the binding affinity of **L3** for iron. The p*K*_b of benzimidazole is also a better match than that of benzoxazole to the p*K*_b of histidine (p*K*_b ≈ 8.0). From a biomimetic point of view, **L3** more accurately matches the electronic properties of the coordinating residues present in the primary coordination sphere in BMM diiron active sites.

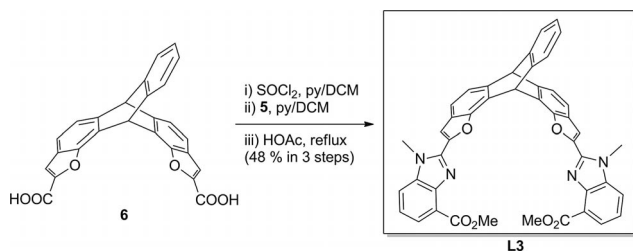
The synthetic route to benzimidazole ligand **L3** requires preparation of methyl 2-amino-3-(methylamino)benzoate (**5**), which was obtained by the route depicted in Scheme 1. Although **5** has an apparently simple structure, differentiation of its two nitrogen atoms by selective protection of nitrogen at the 3-position with a methyl group is a synthetic challenge. For instance, the direct functionalization of 2,3-diaminobenzoate by methylation or reductive amination would not be selective, giving low yields of the desired products and requiring difficult purification protocols. Although a procedure to replace the chlorine atom in 3-chloro-2-nitrobenzoic acid with methylamine under high pressure has been reported,^[45] we obtained a mixture of compounds by

this method. After performing a tedious recrystallization step, the product was isolated in very low yield. Therefore, this reaction is not practical for large-scale synthesis. To prepare large quantities of the desired diamine compound **5**, several synthetic pathways were explored, ultimately leading to the discovery of an efficient route. The optimized synthesis of diamine **5** is delineated in Scheme 1. Methyl 3-chloro-2-nitrobenzoate (**1**) can be readily prepared from 3-chloro-2-nitrobenzoic acid in 99% yield, using diazomethane generated from Diazald and 10% aq. NaOH in ethanol. A C–N bond coupling reaction of **1** with *N*-methylacetamide was achieved under Lindenschmidt's conditions, Pd(TFA)₂, BINAP, and Cs₂CO₃.^[46] Methyl 3-(*N*-methylacetamido)-2-nitrobenzoate (**2**) was obtained in high yield (82%) on a large scale. Next, hydrolysis of both the ester and amide groups with excess 10% aq. NaOH in ethanol at 80 °C gave 3-(methylamino)-2-nitrobenzoic acid (**3**). Crude acid **3** was then treated with diazomethane to yield methyl 3-(methylamino)-2-nitrobenzoate (**4**) in 95% yield over two steps from **2**. Lastly, hydrogenation of **4** afforded methyl 2-amino-3-(methylamino)benzoate (**5**) in 95% yield. This five-step synthesis of diamine **5** is efficient, high-yielding (73% overall yield), and can be readily scaled up. Moreover, this approach can be utilized for the synthesis of diamine **5** analogs, facilitating the preparation of other **L3** ligand variants.



Scheme 1. Diaminobenzoate synthesis.

With diamine **5** in hand, the amide coupling reaction between **5** and **6** was carried out (Scheme 2).^[36] In contrast to the synthesis of benzoxazole ligand **L1**, the coupling reaction between diacid **6** and diamine **5** generated an inseparable mixture of compounds. Because compound **5** contains two different amine functionalities, several different products can be obtained depending on which amine group reacts to form the amide bond. The final cyclization step,



Scheme 2. Synthesis of ligand **L3**.

however, is expected to yield the same product regardless of which amide bonds were present. Hence, cyclization of the crude mixture in glacial acetic acid afforded the desired ligand, **L3**, as the major product in 48% yield from diacid **6**.

Three-Component Titration Experiments

With diester ligand **L3** in hand, we next explored its iron coordination chemistry. Because the active site of sMMOH contains two iron atoms surrounded by two nitrogen and four carboxylate donors, we wished to reproduce this stoichiometry in our model compounds. Although ligand **L3** is designed to bind to two iron atoms, external carboxylate ligands are needed to complete the coordination sphere of the diiron core. To determine the ratio of iron(II) and external carboxylates that the **L3** platform can accommodate, we carried out a series of UV/Vis spectrophotometric titrations.^[42,47,48]

We first examined the coordination behavior of ligand **L3** with an iron(II) salt in the absence of an external carboxylate ligand. As shown in Figure 3, when various aliquots of Fe(OTf)₂ were added to a solution of **L3** in dichloromethane, the absorption band at 345 nm decreased concomitantly with increases at 365 and 386 nm, features that are characteristic of an Fe–O(H)–Fe species. The appearance of an isosbestic point at 308 nm indicates a single-step conversion between two different species, suggesting that the apo **L3** ligand binds to iron(II). These spectroscopic features did not change significantly when greater than 2.0 equiv. of Fe(OTf)₂ were added (Figure 3, inset). Although the exact iron-to-ligand ratio cannot be determined with certainty, these titration results reveal that ligand **L3** can bind to more than one iron atom. This result is encouraging given that some other ligand systems developed in our laboratory could only produce complexes with a 1:1 iron-to-ligand ratio.^[38,42]

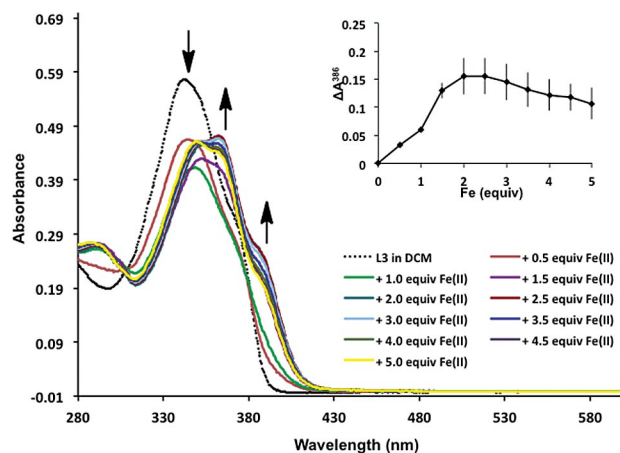


Figure 3. UV/Vis absorption spectra obtained from addition of Fe(OTf)₂ (0.5 equiv.) to **L3** (10 μM in dichloromethane). The inset shows the absorbance changes at 386 nm, where the error bars for each data point were calculated from triplicate experiments.

We next sought to determine the stoichiometry of carboxylate binding to the diiron complex of **L3**. To a premixed

solution containing **L3** and $\text{Fe}(\text{OTf})_2$ in a 1:2 ratio, the carboxylate $\text{Et}_3\text{NH}(\text{O}_2\text{CAr}^{\text{Tol}})$ [triethylammonium 2,6-bis(*p*-tolyl)benzoate] was added in small portions and binding was monitored by UV/Vis absorption spectroscopy. The addition of up to 1.0 equiv. of $\text{Et}_3\text{NH}(\text{O}_2\text{CAr}^{\text{Tol}})$ resulted in an increase in absorption bands at 365 and 386 nm. Figure 4a shows a plot of the absorption changes at 386 nm upon addition of $\text{Et}_3\text{NH}(\text{O}_2\text{CAr}^{\text{Tol}})$ to **L3**. When greater than 1.0 equiv. of the carboxylate were introduced, the band at 386 nm decreased while another appeared at 345 nm. The band at 345 nm arises from the free ligand, **L3**. We could reason that the addition of a large excess of carboxylate leads to extrusion of iron from **L3**, forming iron carboxylate complexes and free **L3**.^[18,19] These studies suggested that only 1.0 equiv. of carboxylate should be utilized to prepare diiron complexes supported by **L3**.

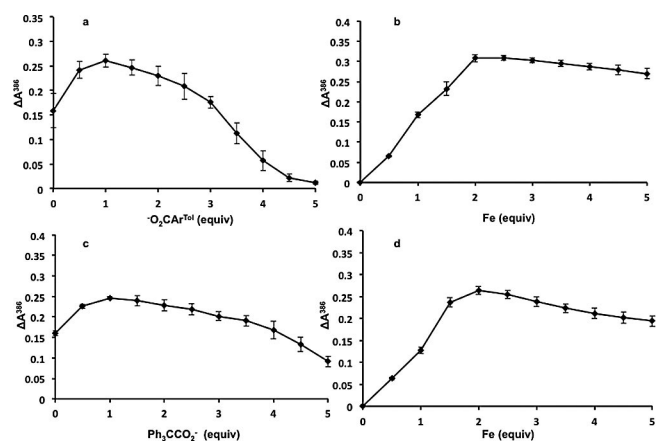


Figure 4. UV/Vis titration experiments: (a) addition of $\text{Et}_3\text{NH}(\text{O}_2\text{CAr}^{\text{Tol}})$ to a premixed solution of **L3** ($10\ \mu\text{M}$ in dichloromethane) and $\text{Fe}(\text{OTf})_2(\text{MeCN})_2$ (1:2); (b) addition of $\text{Fe}(\text{OTf})_2(\text{MeCN})_2$ to a premixed solution of **L3** ($10\ \mu\text{M}$ in dichloromethane) and $\text{Et}_3\text{NH}(\text{O}_2\text{CAr}^{\text{Tol}})$ (1:1); (c) addition of $\text{Na}(\text{O}_2\text{CCPh}_3)$ to a premixed solution of **L3** ($10\ \mu\text{M}$ in dichloromethane) and $\text{Fe}(\text{OTf})_2(\text{MeCN})_2$ (1:2); (d) addition of $\text{Fe}(\text{OTf})_2(\text{MeCN})_2$ to a premixed solution of **L3** ($10\ \mu\text{M}$ in dichloromethane) and $\text{Na}(\text{O}_2\text{CCPh}_3)$ (1:1). Each plot shows the absorbance changes at 386 nm. The error bars for each data point were calculated from triplicate experiments.

To investigate whether the ratio of iron, external carboxylates, and **L3** depends on the order of addition, a final set of titrations was carried out by adding $\text{Fe}(\text{OTf})_2$ to a premixed solution of **L3** and $\text{Et}_3\text{NH}(\text{O}_2\text{CAr}^{\text{Tol}})$ (1:1). Figure 4b shows a plot of the UV/Vis absorbance changes at 386 nm following addition of $\text{Fe}(\text{OTf})_2$ to **L3**/ $\text{Et}_3\text{NH}(\text{O}_2\text{CAr}^{\text{Tol}})$. The absorbance increased linearly until 2.0 equiv. of $\text{Fe}(\text{OTf})_2$ were added. Treatment with additional equivalents of $\text{Fe}(\text{OTf})_2$ led to a slight decrease in the absorption at 386 nm, which is most likely a result of competitive binding of excess Fe^{II} to the external carboxylate groups.

Similar titration experiments were carried out with sodium 2,2,2-triphenylacetate instead of 2,6-bis(*p*-tolyl)benzoate and yielded comparable results (Figure 4c and 4d). Taken together, these studies suggest that at least one external carboxylate can bind to a diiron-**L3** complex.

Iron Complexes of **L3**

By combining **L3**, carboxylate, and iron(II) in a 1:1:2 ratio, as determined to be optimal for diiron complex formation according to the titration experiments described above, crystals of $[\text{Fe}_2\text{L3}(\mu\text{-OH})(\mu\text{-O}_2\text{CR})(\text{OTf})_2]$ [where $\text{R} = \text{Ar}^{\text{Tol}}$ (**7**) or Ph_3C (**8**)] were obtained in moderate yield. Figures 5 and 6 depict the structures for **7** and **8**, respectively, along with relevant bond metrics. Compounds **7** and **8** are structural analogs, differing only in the identity of their bridging carboxylate ligand. Each iron center is five-coordinate, comprising *O*-ester and *N*-benzimidazole groups from **L3**, a terminal triflate (OTf^-), a bridging hydroxide, and a bridging carboxylate. The Fe–O distances of the triflate ligands vary between 2.184 and 2.284 Å and are longer than other Fe–O distances in these structures (Figures 5 and 6). Additionally, one of the terminal triflate ligands forms a hydrogen-bonding interaction with the bridging hydroxide.

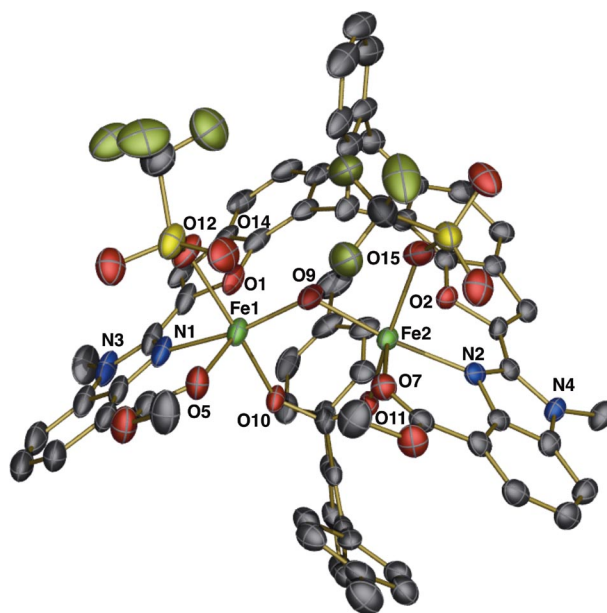


Figure 5. Molecular structure of $[\text{Fe}_2\text{L3}(\mu\text{-OH})(\mu\text{-O}_2\text{CAr}^{\text{Tol}})(\text{OTf})_2]$ (**7**) with 50% probability thermal ellipsoids and a partial numbering scheme (hydrogen atoms and solvent molecules are omitted for clarity). Iron, green; carbon, gray; oxygen, red; nitrogen, blue; sulfur, yellow; fluorine, yellow-green. Selected bond lengths (Å) and angles ($^\circ$): Fe1–N1, 2.084(6); Fe2–N2, 2.100(6); Fe1–O5, 2.091(6); Fe2–O7, 2.122(5); Fe1–O10, 2.074(5); Fe2–O11, 2.068(5); Fe1–O9, 1.943(5); Fe2–O9, 1.962(5); Fe1–O12, 2.284(3); Fe2–O15, 2.212(6); Fe1–O9–Fe2, 126.5(3); O9–Fe1–O10, 97.9(2); O9–Fe2–O11, 95.0(2); O9–Fe1–N1, 167.3(3); O9–Fe2–N2, 168.1(2); O10–Fe1–O12, 170.50(16); O11–Fe2–O15, 163.6(2).

Compounds **7** and **8** are also structurally similar to the diiron complex derived from the bis(benzoxazole) ligand **L1**. Despite having an identical set of ligands, the diiron complex of **L1**, $[\text{Fe}_2\text{L1}(\mu\text{-OH})(\mu\text{-O}_2\text{CAr}^{\text{Tol}})(\text{OTf})_2]$ (**9**),^[36] exhibits some notable differences from benzimidazole analogs **7** and **8**. A comparison of relevant structural parameters of these three complexes is provided in Table 1. Even though a more strongly donating benzimidazole ligand is present in **7** and **8**, the Fe–N distances of approximately 2.1 Å are similar to those in the benzoxazole structure. The

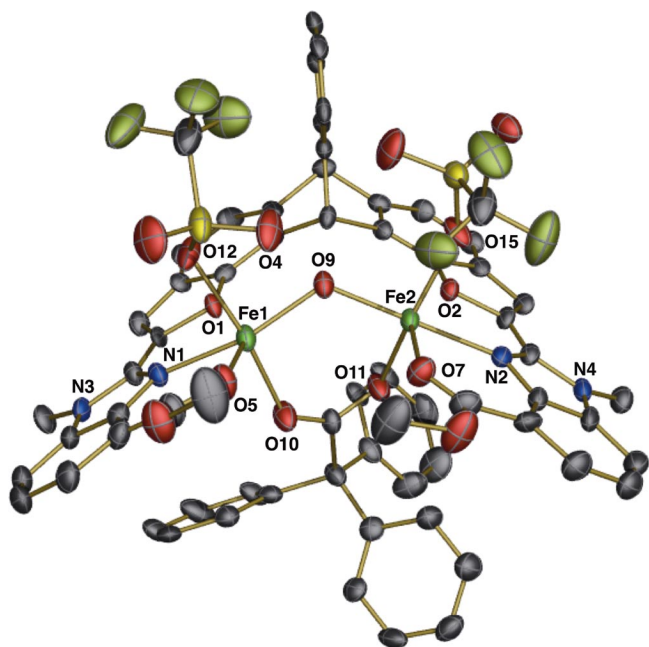


Figure 6. Molecular structure of $[\text{Fe}_2\text{L}_3(\mu\text{-OH})(\mu\text{-O}_2\text{CCPh}_3)(\text{OTf})_2]$ (**8**) with 50% probability thermal ellipsoid and a partial numbering scheme (hydrogen atoms and solvent molecules are omitted for clarity). Iron, green; carbon, gray; oxygen, red; nitrogen, blue; sulfur, yellow; fluorine, yellow-green. Selected bond lengths (Å) and angles ($^\circ$): Fe1–N1, 2.106(4); Fe2–N2, 2.113(4); Fe1–O5, 2.133(4); Fe2–O7, 2.128(4); Fe1–O10, 2.073(4); Fe2–O11, 2.062(4); Fe1–O9, 1.961(4); Fe2–O9, 1.953(4); Fe1–O12, 2.230(4); Fe2–O15, 2.184(4); Fe1–O9–Fe2, 123.3(2); O9–Fe1–O10, 97.04(15); O9–Fe2–O11, 93.23(15); O9–Fe1–N1, 158.25(17); O9–Fe2–N2, 177.68(17); O10–Fe1–O12, 170.52(15); O11–Fe2–O15, 159.51(16).

other Fe–L distances are similar as well. The parameter τ [$\tau = (\beta - \alpha)/60$, $\beta > \alpha$], provides an assessment of a five-coordinate structure having a geometry between that of an idealized trigonal bipyramid ($\tau = 1$) and a square pyramid ($\tau = 0$).^[49–51] The τ values for the iron atoms in **7–9** are summarized in Table 1. The two iron atoms of **7** attain a nearly perfect square-pyramidal coordination geometry as evidenced by τ values close to 0 (0.05 and 0.08). The iron atoms of **8** and **9** exhibit a higher degree of distortion toward trigonal-bipyramidal stereochemistry. The τ values for **8** are 0.20 and 0.30, whereas those for **9** are 0.30 and 0.41. The greater distortion of **9** toward trigonal-pyramidal geometry may be a consequence of the weaker donor ability of the benzoxazole nitrogen atoms. Although compounds **7** and **8** have a hydroxido-bridged diiron(II) core, similar electronic effects may be at play in determining the coordination geometry. The Fe \cdots Fe separations of **8** and **9** are 3.44 Å, whereas in **7** the distance is slightly elongated, 3.49 Å. Although minimal, this structural difference may be associated with the greater degree of square-pyramidal character of **7** relative to those of **8** and **9**. Another significant difference between benzimidazole structures **7** and **8** and benzoxazole structure **9** is the presence of weak interactions at the available remaining coordination sites at the Fe^{II} centers and the oxygen atoms of the furan ring (O1 and O2). In **9**, these Fe–O distances are 2.987 and 3.060 Å

(Table 1). For **7** and **8** these distances contract significantly. The Fe–O distances in these complexes range from 2.609 to 2.859 Å. These shorter distances could in part be due to more rigorous square-pyramidal geometry enforced by the benzimidazole ligands.

Table 1. Selected distances (Å), angles ($^\circ$), and values of the geometric parameter τ in complexes **7–9**. Numbers in parentheses are standard deviations in the last digit(s).

	7	8	9
Fe1 \cdots Fe2	3.4867(14)	3.4445(10)	3.4436(13)
N1 \cdots N2	7.336(8)	7.232(6)	7.321(8)
Fe1 \cdots O1	2.690(6)	2.859(3)	2.987(5)
Fe2 \cdots O2	2.696(5)	2.609(4)	3.060(5)
O1 \cdots O2	5.134(7)	5.168(4)	5.075(6)
Fe–OH–Fe	126.5(3)	123.3(2)	124.4(3)
τ (Fe1)	0.058(6)	0.205(4)	0.303(5)
τ (Fe2)	0.075(5)	0.303(4)	0.408(5)

The dinucleating ligand conformations are similar for structures **7–9** (Table 1). The distance between nitrogen donor atoms (N1 \cdots N2) varies from 7.232 to 7.336 Å, whereas the distances between furan oxygen atoms (O1 \cdots O2) fall between 5.075 and 5.168 Å. These small structural variations reflect the preorganization of the triptycene backbone. Rotation about the C–C bond between the benzofuran backbone and the benzoxazole or benzimidazole arms of the ligands will allow for some structural flexibility, however, as may be required for efficient metal coordination. These dihedral angles in **9** are 2.69 and 3.76 $^\circ$ for the two arms. In the benzimidazole structures the analogous dihedral angles range from 4.47 to 7.70 $^\circ$, which indicates somewhat greater distortion from coplanarity of the two π systems. This subtle change in dihedral angle may be a consequence of the preferred coordination geometry of the benzimidazole compared to that of the benzoxazole structures.

Mössbauer Spectra of Complexes **7** and **8**

Zero-field ^{57}Fe Mössbauer spectra of polycrystalline samples of complexes **7** and **8** were recorded at 77 K. Both spectra show a single quadrupole doublet, as shown in Figure 7 for **7**. Table 2 lists the parameters of complexes **7** and **8**. The isomer shift (δ) of **7** is 1.218 mm s $^{-1}$ and the quadrupole splitting (ΔE_Q) is 1.960 mm s $^{-1}$. These parameters are characteristic of high-spin diiron(II) complexes. The values compare favorably to those for the benzoxazole analog **9**, which has an isomer shift of 1.214 mm s $^{-1}$ and a quadrupole splitting of 1.925 mm s $^{-1}$. In addition, the isomer shift (δ) of **8** is 1.224 mm s $^{-1}$ and the quadrupole splitting (ΔE_Q) is 2.064 mm s $^{-1}$. Although the solid-state structures indicate slightly different coordination geometries at the two iron centers, these differences have a minimal effect on electronic properties, as reflected by a single isomer shift.

Table 2. Mössbauer fits for complexes **7** and **8**.

	7	8
Isomer shift δ (mm s $^{-1}$)	1.218	1.224
Quadrupole splitting ΔE_Q (mm s $^{-1}$)	1.960	2.064

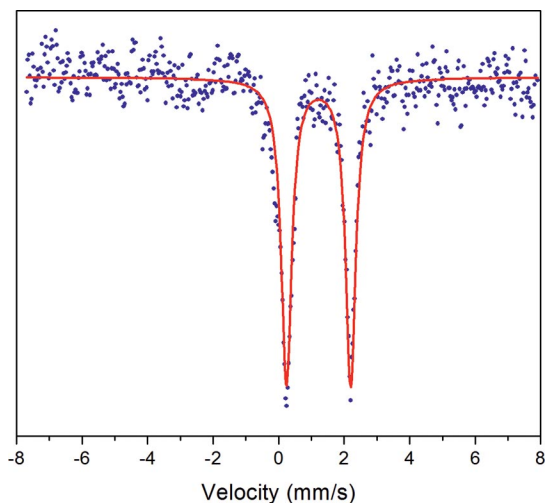


Figure 7. Zero-field ^{57}Fe Mössbauer spectrum of complex **7** recorded at 77 K. The red line is the best fit to the data.

Conclusions

With the goal of increasing the electron-donating properties of our first-generation triptycene-based ligand, **L1**, we designed and synthesized an analogous ligand, **L3**, which introduces a more basic benzimidazole nitrogen donor in place of the benzoxazole nitrogen donor of **L1**. Ligand **L3** was obtained in a 15-step convergent synthesis. Titration experiments were conducted to determine the appropriate combination of iron(II), carboxylate, and **L3** required to assemble a diiron complex. The X-ray crystal structures of two such carboxylate-bridged diiron complexes reveal that **L3** binds to a diiron unit in a fashion similar to that of **L1**. Complexes of **L3** exhibit some structural differences in comparison to those of **L1**. Most notably, diiron complexes **7** and **8** feature coordination geometries closer to square-pyramidal and a close Fe–O interaction with benzofuran backbone. The iron oxidation states of the new complexes were confirmed by utilizing Mössbauer spectroscopy. Ongoing work is focused on the hydrolysis of the ester moieties of **L3** to form a more biomimetic carboxylate ligand.

Experimental Section

General Methods and Materials: Reagents purchased from TCI, Aldrich Chemical Co., and Alfa Aesar were used as received, unless otherwise noted. The synthesis of compound **6** was described previously.^[36] Column chromatography was carried out with Silicycle 60 Å, ultrapure silica gel. ^1H and ^{13}C NMR spectra were recorded with a 300 MHz or 500 MHz Varian Mercury spectrometer. IR spectra were measured with a ThermoNicolet Avatar 360 spectrophotometer controlled by the OMNIC software. Low-resolution electrospray ionization mass spectra were acquired with an Agilent Technologies 1100 series LC-MSD trap. High-resolution mass spectra were obtained with a Bruker Daltonics APEXIV 4.7 Tesla Fourier Transform ion cyclotron resonance mass spectrometer (FT-ICRMS) at the MIT Department of Chemistry Instrument Facility (DCIF).

X-ray Diffraction Studies

Single crystals suitable for X-ray analysis were coated with Paratone-N oil, suspended in a small fiber loop, and placed in a cooled dry N_2 gas stream on a Bruker APEX CCD X-ray diffractometer. Data were acquired by using graphite monochromated Mo-K_α radiation ($\lambda = 0.71073 \text{ \AA}$) at 100(2) K and a combination of ϕ and ω scans traversing their respective scanning angles at 0.5° increments for ω scans and 0.45° increments for ϕ scans. Data collection, indexing, reduction, and final unit cell refinement procedures were carried out by using APEX2; absorption corrections were applied by using the program SADABS. All structures were solved with direct methods with SHELXS^[52] and refined against F^2 on all data by full-matrix least-squares with SHELXL,^[53] following established refinement strategies.^[54] Data collection and refinement parameters are summarized in Table 3, and specific refinement details are given below.

For compound **7**, the crystal diffracted only to a maximum θ value of 23.4° . A molecule of dichloromethane and diethyl ether are present in the asymmetric unit, along with the diiron complex. The diethyl ether molecule was refined with similarity restraints on the thermal ellipsoids and carbon–carbon bond lengths. The triflate ligand coordinated to Fe1 is disordered, adopting two orientations. The disorder was modeled by restraining both components to have similar bond lengths and thermal ellipsoid parameters. The occupancy factors of the disordered components were refined, constraining the sum of the occupancy factors to unity. The major component refined to an occupancy value of 0.68. The hydrogen atom of the bridging hydroxido ligand was located on a difference Fourier map, and the O–H distance was constrained to 0.84 \AA . The thermal ellipsoid of the hydrogen atom was constrained to be 1.5 times that of the oxygen atom to which it is attached. At the final stages of refinement, a large residual electron density peak of 4.38 e \AA^{-3} remained. This peak is located 0.85 \AA from H10, an atom on the triptycene backbone. The origin of this large residual electron density remains uncertain, but may reflect series termination errors owing to the low resolution and intensity of the data set.

Crystals of **8** diffracted well. The asymmetric unit consists of the diiron complex and a molecule of dichloromethane. The latter is disordered, having two orientations that were refined with similarity restraints on both the bond lengths and thermal ellipsoids. The major component of this disorder refined to an occupancy factor of 0.53. The hydrogen atom of the bridging hydroxido ligand was located on a difference Fourier map and refined as described for **7**. The absolute structure (Flack) parameter, refined by using the racemic twin law, converged to a value of 0.395 with a standard uncertainty of 0.019, indicating that the crystal is most likely a twin with a minor domain of the opposite absolute structure comprising approximately 40% of the crystal.

CCDC-909410 (for **7**) and -909411 (for **8**) contain the supplementary crystallographic data for this paper. These data can be obtained free of charge from The Cambridge Crystallographic Data Centre via www.ccdc.cam.ac.uk/data_request/cif.

^{57}Fe Mössbauer Spectroscopy: Mössbauer spectra were recorded with a MSI spectrometer (WEB Research Co.) with a ^{57}Co source in a Rh matrix maintained at room temperature. Solid samples were prepared by suspension in Apiezon M grease and placed in a nylon sample holder. Data were acquired at 77 K, and the isomer shift (δ) values are reported with respect to metallic iron that was used for velocity calibration at room temperature. The spectra were fit to Lorentzian lines by using the WMOSS plot and fit program (WEB Research Co.).

Table 3. Crystal data and structure refinement for complexes **7** and **8**.

	7 ·(CH ₂ Cl ₂)·(Et ₂ O)	8 ·(CH ₂ Cl ₂)
Empirical formula	C ₇₂ H ₆₀ Cl ₂ F ₆ Fe ₂ N ₄ O ₁₆ S ₂	C ₆₇ H ₄₈ Cl ₂ F ₆ Fe ₂ N ₄ O ₁₅ S ₂
Formula weight	1597.96	1509.81
Temperature (K)	100(2)	100(2)
Wavelength (Å)	0.71073	0.71073
Crystal system	monoclinic	orthorhombic
Space group	<i>P</i> 2 ₁ / <i>c</i>	<i>P</i> 2 ₁ 2 ₁ 2 ₁
Unit cell dimensions		
<i>a</i> (Å)	19.9244(14)	16.0657(9)
<i>b</i> (Å)	20.6794(15)	19.7408(11)
<i>c</i> (Å)	19.7602(14)	19.9989(11)
β (°)	118.8530(10)	
Volume (Å ³)	7131.0(9)	6342.6(6)
<i>Z</i>	4	4
<i>D</i> _{calcd.} (g cm ⁻³)	1.488	1.581
Absorption coefficient (mm ⁻¹)	0.627	0.698
<i>F</i> (000)	3280	3080
Crystal size (mm ³)	0.40 × 0.10 × 0.10	0.20 × 0.14 × 0.06
Theta range (°)	1.55 to 23.38	1.63 to 25.14
Index ranges	-22 ≤ <i>h</i> ≤ 22 -23 ≤ <i>k</i> ≤ 23 -22 ≤ <i>l</i> ≤ 22	-18 ≤ <i>h</i> ≤ 19 -23 ≤ <i>k</i> ≤ 23 -23 ≤ <i>l</i> ≤ 23
Reflections collected	97291	101906
Independent reflections	10347 [<i>R</i> (int) = 0.0640]	11325 [<i>R</i> (int) = 0.1103]
Maximum θ (°)	23.38	25.14
Completeness to 2 θ (%)	99.6	99.8
Absorption correction	semiempirical from equivalents	semiempirical from equivalents
Max. and min. transmission	0.9400 and 0.7876	0.9593 and 0.8729
Refinement method	full-matrix least-squares on <i>F</i> ²	full-matrix least-squares on <i>F</i> ²
Data/restraints/parameters	10347/244/946	11325/56/913
Goodness-of-fit on <i>F</i> ²	1.054	1.047
Final <i>R</i> indices [<i>I</i> > 2 σ (<i>I</i>)]	<i>R</i> ₁ = 0.0917, <i>wR</i> ₂ = 0.2417	<i>R</i> ₁ = 0.0569, <i>wR</i> ₂ = 0.1190
<i>R</i> indices (all data)	<i>R</i> ₁ = 0.1204, <i>wR</i> ₂ = 0.2682	<i>R</i> ₁ = 0.0860, <i>wR</i> ₂ = 0.1314
Largest diff. peak and hole (e Å ⁻³)	4.375 and -0.698	1.029 and -0.435

Methyl 3-Chloro-2-nitrobenzoate (1): Diazomethane, CH₂N₂, generated from Diazald and 10% NaOH in EtOH, was bubbled into a suspension of 3-chloro-2-nitrobenzoic acid (10.0 g, 50 mmol) in Et₂O (250 mL) under a steam of nitrogen. The reaction was monitored by TLC until completion. The resulting solution was passed through a short pad of silica gel. The product, which was retained on the column, was eluted with acetone. After rotary evaporation of the acetone eluate, methyl 3-chloro-2-nitrobenzoate (**1**) was obtained as a white solid. Yield 10.6 g (99%). Melting point: 105–106 °C. ¹H NMR (300 MHz in CDCl₃): δ = 3.90 (s, 3 H), 7.53 (t, *J* = 8.1 Hz, 1 H), 7.70 (dd, *J*₁ = 1.5, *J*₂ = 8.1 Hz, 1 H), 7.97 (dd, *J*₁ = 1.5, *J*₂ = 7.8 Hz, 1 H) ppm. ¹³C NMR (75 MHz in CDCl₃): δ = 53.49, 124.43, 126.38, 129.83, 130.15, 130.92, 134.91, 162.68 ppm. IR (KBr): $\tilde{\nu}$ = 3107, 3066, 2957, 2906, 2850, 1732, 1552, 1444, 1384, 1288, 1216, 1172, 978, 853, 765, 718 cm⁻¹. LRMS (ESI+) *m/z*: 237.9, 239.9 [M + Na]⁺ (calcd. for C₈H₆ClNNaO₄: 238.0, 240.0).

Methyl 3-(*N*-Methylacetamido)-2-nitrobenzoate (2): A flask containing methyl 3-chloro-2-nitrobenzoate (**1**) (8.6 g, 40 mmol), Cs₂CO₃ (15.6 g, 48 mmol, 1.2 equiv.), Pd(TFA)₂ (TFA = trifluoroacetate) (664 mg, 5 mol-%), and BINAP (1.25 g, 5 mol-%) was evacuated and back-filled with nitrogen three times. *N*-Methylacetamide (4.1 g, 56 mmol, 1.4 equiv.) was added with a syringe, followed by addition of anhydrous toluene (240 mL). The resulting mixture was heated at 80–85 °C for three days under a nitrogen atmosphere. The resulting black solution was cooled to room temperature. Water (300 mL) was added, and the resulting mixture was extracted with EtOAc (4 × 100 mL). The combined organic layers

were washed with 10% aq. HCl (50 mL) and brine (50 mL), dried with Na₂SO₄, filtered, and concentrated to dryness. Flash column chromatography of the resulting residue (dichloromethane/acetone = 1:0–4:1) gave methyl 3-(*N*-methylacetamido)-2-nitrobenzoate (**2**) as a yellow solid. Yield 8.2 g (82%). Melting point: 120–122 °C. ¹H NMR (300 MHz in CDCl₃): δ = 1.81 (s, 3 H), 3.14 (s, 3 H), 3.91 (s, 3 H), 7.55 (dd, *J*₁ = 1.5, *J*₂ = 7.8 Hz, 1 H), 7.68 (t, *J* = 7.8 Hz, 1 H), 8.10 (dd, *J*₁ = 1.5, *J*₂ = 7.8 Hz, 1 H) ppm. ¹³C NMR (75 MHz in CDCl₃): δ = 22.23, 37.10, 53.51, 124.36, 130.13, 131.61, 131.82, 134.48, 136.67, 162.79, 170.38 ppm. IR (KBr): $\tilde{\nu}$ = 3068, 3034, 2958, 2851, 1738, 1671, 1546, 1442, 1384, 1355, 1290, 1201, 1164, 1001, 859, 834, 769, 701, 637, 606, 586, 573 cm⁻¹. HRMS (ESI+) *m/z* = 253.0809 [M + H]⁺ (calcd. for C₁₁H₁₃N₂O₅: 253.0824).

3-(Methylamino)-2-nitrobenzoic Acid (3): A solution of methyl 3-(*N*-methylacetamido)-2-nitrobenzoate (**2**) (8.0 g, 31.7 mmol) in a mixture of 10% aq. NaOH and EtOH (520 mL:200 mL) was heated at 80–85 °C for 10 h. The resulting orange-red solution was cooled to 0 °C. Concentrated HCl was added slowly to adjust the pH to 1.5–2.0. The resulting mixture was extracted with EtOAc (4 × 150 mL). The combined organic layers were washed with brine (30 mL), dried with Na₂SO₄, filtered, and concentrated to dryness. The desired product, 3-(methylamino)-2-nitrobenzoic acid (**3**) (7.2 g), was obtained as a red solid. The crude **3** was used in the next step without further purification. ¹H NMR (500 MHz in CD₃OD): δ = 2.96 (s, 3 H), 6.80 (dd, *J*₁ = 1.5, *J*₂ = 7.5 Hz, 1 H), 7.04 (dd, *J*₁ = 1.5, *J*₂ = 8.5 Hz, 1 H), 7.46 (dd, *J*₁ = 7.5, *J*₂ = 8.5 Hz, 1 H) ppm. ¹³C NMR (125 MHz in CD₃OD): δ = 30.30, 116.78, 116.82, 132.60, 133.43, 135.29, 146.18, 170.80 ppm. IR (KBr): $\tilde{\nu}$ =

3392, 2911, 1700, 1615, 1575, 1512, 1448, 1253, 1180, 1078, 1053, 799, 765 cm⁻¹. HRMS (ESI+) *m/z* = 197.0566 [M + H]⁺ (calcd. for C₈H₉N₂O₄: 197.0562).

Methyl 3-(Methylamino)-2-nitrobenzoate (4): Crude 3-(methylamino)-2-nitrobenzoic acid (**3**) (1 g) was suspended in Et₂O (150 mL). In a well-ventilated hood, diazomethane, generated by slow addition of 10% aq. NaOH to a solution of Diazald (2 equiv.) in EtOH, was bubbled into the ethereal solution under a stream of nitrogen until the reaction was complete, as evaluated by TLC. This reaction was repeated seven times on similar 1 g scales until all of the above crude material was converted. The combined red oil was purified by column chromatography (hexanes/EtOAc = 1:0, 10:1–4:1) to obtain methyl 3-(methylamino)-2-nitrobenzoate (**4**) as a red oil. Yield: 6.0 g (90% in two steps). ¹H NMR (300 MHz in CDCl₃): δ = 3.00 (d, *J* = 4.8 Hz, 3 H), 3.88 (s, 3 H), 6.75 (dd, *J*₁ = 1.2, *J*₂ = 7.2 Hz, 1 H), 6.91 (d, *J* = 8.7 Hz, 1 H), 7.42 (dd, *J*₁ = 7.2, *J*₂ = 8.7 Hz, 1 H), 7.54 (br. s, 1 H) ppm. ¹³C NMR (75 MHz in CDCl₃): δ = 30.20, 53.28, 115.59, 116.11, 130.16, 132.27, 134.77, 145.60, 168.08 ppm. IR (KBr): ν̄ = 3398, 3002, 2952, 2839, 1732, 1613, 1573, 1511, 1446, 1358, 1280, 1208, 1119, 1079, 1054, 983, 853, 792, 754, 704, 547, 482 cm⁻¹. HRMS (ESI+) *m/z* = 211.0714 [M + H]⁺ (calcd. for C₉H₁₁N₂O₄: 211.0719).

Methyl 2-Amino-3-(methylamino)benzoate (5): A mixture of methyl 3-(methylamino)-2-nitrobenzoate (**4**) (2.0 g, 9.5 mmol) and 10% Pd/C (100 mg, 5% w/w) in EtOAc/MeOH (50 mL/25 mL) was hydrogenated with hydrogen from a balloon for 60 h. The catalyst was removed by filtration through filter paper, and the resulting solution was concentrated to dryness. Flash column chromatography of the residue (hexanes/EtOAc = 10:1–2:1) gave methyl 2-amino-3-(methylamino)benzoate (**5**) as a brown solid. Yield 1.43 g (83%). Melting point: 53–55 °C. ¹H NMR (500 MHz in CDCl₃): δ = 2.87 (s, 3 H), 3.87 (s, 3 H), 4.50–5.10 (br. s, 3 H), 6.73 (dd, *J*₁ = 7.5, *J*₂ = 8.5 Hz, 1 H), 6.80 (dd, *J*₁ = 1.0, *J*₂ = 7.5 Hz, 1 H), 7.45 (dd, *J*₁ = 1.0, *J*₂ = 8.0 Hz, 1 H) ppm. ¹³C NMR (125 MHz in CDCl₃): δ = 31.56, 51.78, 111.69, 115.29, 117.40, 121.17, 138.04, 141.13, 169.35 ppm. IR (KBr): ν̄ = 3541, 3482, 3404, 3273, 2948, 2858, 2805, 1677, 1622, 1570, 1493, 1469, 1455, 1438, 1384, 1287, 1239, 1190, 1087, 811, 745 cm⁻¹. HRMS (ESI+) *m/z* = 181.0974 [M + H]⁺ (calcd. for C₉H₁₃N₂O₂: 181.0977).

Ligand L3: Pyridine (646 μL, 8 mmol, 40 equiv.) was added to a suspension of diacid **6** (84.4 mg, 0.2 mmol) in anhydrous dichloromethane (80 mL) under a nitrogen atmosphere. Thionyl chloride (584 μL, 8 mmol, 40 equiv.) was added, and the resulting solution was stirred at room temperature for 60 h. The volatiles were removed by rotary evaporation, and the residue was dried further under high vacuum for 8 h. To the resulting solid were added anhydrous dichloromethane (40 mL) and pyridine (646 μL, 8 mmol, 40 equiv.), followed by methyl 2-amino-3-(methylamino)benzoate (**5**) (72 mg, 0.4 mmol, 2 equiv.). The resulting light-brown solution was stirred at room temperature for 30 h, after which all the volatiles were removed under vacuum. This crude material was used in the next step without further purification. A solution of the crude solid in HOAc (20 mL) was heated at reflux for 1 h. The acetic acid was removed under reduced pressure. The residue, purified by flash column chromatography with silica gel neutralized by Et₃N (dichloromethane/EtOAc = 20:1–6:1), gave ligand **L3** as a pale yellow solid. Yield 68 mg (48% in 3 steps). Melting point: 333–335 °C. ¹H NMR (500 MHz in CDCl₃): δ = 4.08 (s, 3 H), 4.33 (s, 3 H), 5.75 (s, 1 H), 6.87 (s, 1 H), 7.03–7.08 (m, 2 H), 7.28 (d, *J* = 7.5 Hz, 2 H), 7.37 (dd, *J*₁ = 7.5, *J*₂ = 8.0 Hz, 2 H), 7.44 (d, *J* = 8.0 Hz, 2 H), 7.48–7.51 (m, 1 H), 7.60–7.64 (m, 4 H), 7.66–7.69 (m, 1 H), 8.02 (d, *J* = 7.5 Hz, 2 H) ppm. ¹³C NMR (125 MHz in CDCl₃): δ

= 32.52, 41.89, 52.61, 54.60, 111.30, 114.40, 118.79, 120.35, 121.30, 122.96, 124.12, 124.51, 125.47, 125.74, 126.10, 126.46, 128.30, 137.52, 141.59, 143.84, 145.94, 146.10, 146.37, 146.62, 150.57, 166.70 ppm. IR (KBr): ν̄ = 3127, 3065, 2947, 2839, 1711, 1636, 1606, 1449, 1384, 1294, 1254, 1207, 1118, 1061, 836, 752, 713, 680 cm⁻¹. HRMS (ESI+) *m/z* = 711.2244 [M + H]⁺ (calcd. for C₄₄H₃₁N₄O₆: 711.2244).

[Fe₂L3(μ-OH)(μ-O₂CAr^{Tol})(OTf)₂] (7): In a nitrogen-filled glovebox, a solution of 2,6-bis(*p*-tolyl)benzoic acid (HO₂CAr^{Tol}) (12.8 mg, 0.042 mmol, 1.0 equiv.) in THF (2 mL) was added to a solution of Fe(OTf)₂(MeCN)₂ (36.9 mg, 0.085 mmol, 2.0 equiv.) in MeCN (2 mL), followed by addition of wet Et₃N (11.7 μL, 0.085 mmol, 2.0 equiv.). The mixture was stirred at room temperature for 5 min. Ligand **L3** (30 mg, 0.042 mmol) dissolved in dichloromethane (2 mL) was added, and the resulting red solution was stirred for 30 min. All the volatiles were removed under vacuum. The resulting yellow solid was dissolved in dichloromethane/MeOH (2 mL/0.5 mL) to form a dark-red solution. Vapor diffusion of Et₂O into the solution at room temperature over 3 d gave ruby-colored crystals. X-ray structural analysis of a crystal revealed its composition to be [Fe₂L3(μ-OH)(μ-O₂CAr^{Tol})(OTf)₂]·CH₂Cl₂·Et₂O. After washing with Et₂O and drying under vacuum, orange-red crystals were obtained. Yield 22.4 mg (34.8%). IR (KBr): ν̄ = 3491, 3132, 3023, 2961, 2920, 1672, 1620, 1582, 1449, 1409, 1327, 1298, 1237, 1158, 1027, 756, 637 cm⁻¹. [Fe₂L3(μ-OH)(μ-O₂CAr^{Tol})(OTf)₂]·CH₂Cl₂ or C₆₈H₅₀Cl₂F₆Fe₂N₄O₁₅S₂ (1523.87): calcd. C 53.60, H 3.31, N 3.68; found C 53.51, H 3.15, N 3.75.

[Fe₂L3(μ-OH)(μ-O₂CCPh₃)(OTf)₂] (8): In a nitrogen-filled glovebox, a solution of NaO₂CCPh₃ (13.1 mg, 0.042 mmol, 1.0 equiv.) in THF (2 mL) was added to a solution of Fe(OTf)₂(MeCN)₂ (36.9 mg, 0.085 mmol, 2.0 equiv.) in MeCN (2 mL). The mixture was stirred at room temperature for 5 min. A solution of ligand **L3** (30 mg, 0.042 mmol) in dichloromethane (2 mL) was added, and the resulting red solution was stirred for 30 min. All the volatiles were removed under vacuum. The resulting yellow solid was dissolved in dichloromethane/MeOH (2 mL/0.5 mL) to yield a dark-red solution. Vapor diffusion of Et₂O at room temperature over 5 d gave ruby-colored crystals. X-ray structural analysis of this crystal revealed the formula to be [Fe₂L3(μ-OH)(μ-O₂CCPh₃)(OTf)₂]·CH₂Cl₂. After washing with Et₂O and drying under vacuum, orange-red crystals were obtained. Yield 28 mg (43%). IR (KBr): ν̄ = 3514, 3134, 3055, 2963, 2860, 1664, 1597, 1446, 1347, 1305, 1238, 1161, 1030, 877, 754, 637 cm⁻¹. [Fe₂L3(μ-OH)(μ-O₂CCPh₃)(OTf)₂]·(CH₂Cl₂)_{1.25} or C_{67.25}H_{48.5}Cl_{2.5}F₆Fe₂N₄O₁₅S₂ (1531.08): calcd. C 52.76, H 3.19, N 3.66; found C 52.64, H 2.92, N 3.79.

UV/Vis Spectrophotometric Studies: Stock solutions of **L3** (10 μM in dichloromethane), Fe(OTf)₂(MeCN)₂ (4.0 mM in MeCN), Et₃NHO₂CAr^{Tol} (4.0 mM, prepared by mixing equimolar amounts of Et₃N and HO₂CAr^{Tol} in THF), and carboxylate NaO₂CCPh₃ (4.0 mM in MeOH) were prepared in a glovebox.

Reaction of L3 with Fe(OTf)₂(MeCN)₂: A portion of the **L3** stock solution (4.0 mL) was added to a UV/Vis quartz cuvette, sealed tightly with a septum cap, and brought outside the glovebox. Aliquots (5 μL, 0.25 equiv. relative to **L3**) of the Fe(OTf)₂(MeCN)₂ stock solution were added with a 50 μL syringe through the septum seal into the cuvette. The cell was shaken gently before the electronic absorption spectra were recorded.

Reaction of the Carboxylate Ligand with a Mixture of 2.0 equiv. Fe(OTf)₂(MeCN)₂ and L3: Inside a nitrogen-filled glovebox, a mixture containing **L3** stock solution (4 mL) and Fe(OTf)₂(MeCN)₂ stock solution (2.0 equiv.) was added to a UV/Vis quartz cuvette,

sealed tightly with a septum cap, and brought outside the glovebox. Aliquots (5 μL , 1.0 equiv. relative to **L3**) of carboxylate in THF stock solution were added with a 50 μL syringe through the septum seal to the cuvette. The cell was shaken gently before the electronic absorption spectra were recorded.

Reaction of $\text{Fe}(\text{OTf})_2(\text{MeCN})_2$ with a Mixture of 1.0 equiv. Carboxylate and **L3:** Inside a nitrogen-filled glovebox, a mixture containing **L3** stock solution (4 mL) and carboxylate stock solution (1.0 equiv.) was added to a UV/Vis quartz cuvette, sealed tightly with a septum cap, and brought outside the glovebox. Aliquots (5 μL , 0.5 equiv. relative to **L3**) of $\text{Fe}(\text{OTf})_2(\text{MeCN})_2$ in MeCN stock solution were added with a 50 μL syringe through the septum seal to the cuvette. The cell was shaken gently before the electronic absorption spectra were recorded.

Supporting Information (see footnote on the first page of this article): ^1H and ^{13}C NMR spectra.

Acknowledgments

The work was supported by the National Institute of General Medical Sciences (grant GM032134). Ulf-Peter Apfel holds a Feodor Lynen research fellowship from the Alexander von Humboldt Foundation. Justin J. Wilson is the grateful recipient of a David H. Koch Graduate Fellowship. Instrumentation at the MIT Department of Chemistry Instrumentation Facility is maintained with National Institutes of Health (NIH) Grant 1S10RR13886-01.

- [1] M. Merckx, D. A. Kopp, M. H. Sazinsky, J. L. Blazyk, J. Müller, S. J. Lippard, *Angew. Chem.* **2001**, *113*, 2860–2888; *Angew. Chem. Int. Ed.* **2001**, *40*, 2782–2807.
- [2] V. Cafaro, V. Izzo, R. Scognamiglio, E. Notomista, P. Capasso, A. Casbarra, P. Pucci, A. Di Donato, *Appl. Environ. Microbiol.* **2004**, *70*, 2211–2219.
- [3] M. H. Sazinsky, J. Bard, A. Di Donato, S. J. Lippard, *J. Biol. Chem.* **2004**, *279*, 30600–30610.
- [4] M. H. Sazinsky, P. W. Dunten, M. S. McCormick, A. DiDonato, S. J. Lippard, *Biochemistry* **2006**, *45*, 15392–15404.
- [5] A. L. Feig, S. J. Lippard, *Chem. Rev.* **1994**, *94*, 759–805.
- [6] B. J. Wallar, J. D. Lipscomb, *Chem. Rev.* **1996**, *96*, 2625–2657.
- [7] D. M. Kurtz Jr., *J. Biol. Inorg. Chem.* **1997**, *2*, 159–167.
- [8] E. I. Solomon, T. C. Brunold, M. I. Davis, J. N. Kemsley, S.-K. Lee, N. Lehnert, F. Neese, A. J. Skulan, Y.-S. Yang, J. Zhou, *Chem. Rev.* **2000**, *100*, 235–349.
- [9] M. H. Sazinsky, M. Merckx, E. Cadieux, S. Tang, S. J. Lippard, *Biochemistry* **2004**, *43*, 16263–16276.
- [10] A. Åberg, P. Nordlund, H. Eklund, *Nature* **1993**, *361*, 276–278.
- [11] L. Que Jr., *J. Chem. Soc., Dalton Trans.* **1997**, 3933–3940.
- [12] M. Fontecave, S. Ménage, C. Duboc-Toia, *Coord. Chem. Rev.* **1998**, *178–180*, 1555–1572.
- [13] J. Du Bois, T. J. Mizoguchi, S. J. Lippard, *Coord. Chem. Rev.* **2000**, *200–202*, 443–485.
- [14] E. Y. Tshuva, S. J. Lippard, *Chem. Rev.* **2004**, *104*, 987–1011.
- [15] L. Que Jr., W. B. Tolman, *Nature* **2008**, *455*, 333–340.
- [16] S. Friedle, E. Reisner, S. J. Lippard, *Chem. Soc. Rev.* **2010**, *39*, 2768–2779.
- [17] L. H. Do, S. J. Lippard, *J. Inorg. Biochem.* **2011**, *105*, 1774–1785.
- [18] W. B. Tolman, L. Que Jr., *J. Chem. Soc., Dalton Trans.* **2002**, 653–660.
- [19] L. Que Jr., W. B. Tolman, *Angew. Chem.* **2002**, *114*, 1160–1185; *Angew. Chem. Int. Ed.* **2002**, *41*, 1114–1137.
- [20] S. K. Lee, B. G. Fox, W. A. Froland, J. D. Lipscomb, E. Münck, *J. Am. Chem. Soc.* **1993**, *115*, 6450–6451.
- [21] K. E. Liu, A. M. Valentine, D. Wang, B. H. Huynh, D. E. Edmondson, A. Salifoglou, S. J. Lippard, *J. Am. Chem. Soc.* **1995**, *117*, 10174–10185.
- [22] M.-H. Baik, B. F. Gherman, R. A. Friesner, S. J. Lippard, *J. Am. Chem. Soc.* **2002**, *124*, 14608–14615.
- [23] A. Ghosh, F. T. de Oliveira, T. Yano, T. Nishioka, E. S. Beach, I. Kinoshita, E. Münck, A. D. Ryabov, C. P. Horwitz, T. J. Collins, *J. Am. Chem. Soc.* **2005**, *127*, 2505–2513.
- [24] G. Xue, D. Wang, R. De Hont, A. T. Fiedler, X. Shan, E. Münck, L. Que Jr., *Proc. Natl. Acad. Sci. USA* **2007**, *104*, 20713–20718.
- [25] D. Wang, E. R. Farquhar, A. Stubna, E. Münck, L. Que Jr., *Nat. Chem.* **2009**, *1*, 145–150.
- [26] G. Xue, A. T. Fiedler, M. Martinho, E. Münck, L. Que Jr., *Proc. Natl. Acad. Sci. USA* **2008**, *105*, 20615–20620.
- [27] G. Xue, R. De Hont, E. Münck, L. Que Jr., *Nat. Chem.* **2010**, *2*, 400–405.
- [28] A. J. Johansson, H. Noack, P. E. M. Siegbahn, G. Xue, L. Que Jr., *Dalton Trans.* **2009**, 6741–6750.
- [29] R. F. De Hont, G. Xue, M. P. Hendrich, L. Que Jr., E. L. Bominaar, E. Münck, *Inorg. Chem.* **2010**, *49*, 8310–8322.
- [30] G. Xue, A. Pokutsa, L. Que Jr., *J. Am. Chem. Soc.* **2011**, *133*, 16657–16667.
- [31] D. Lee, S. J. Lippard, *J. Am. Chem. Soc.* **1998**, *120*, 12153–12154.
- [32] D. Lee, J. Du Bois, D. Petasis, M. P. Hendrich, C. Krebs, B. H. Huynh, S. J. Lippard, *J. Am. Chem. Soc.* **1999**, *121*, 9893–9894.
- [33] D. Lee, S. J. Lippard, *Inorg. Chem.* **2002**, *41*, 2704–2719.
- [34] D. Lee, B. Pierce, C. Krebs, M. P. Hendrich, B. H. Huynh, S. J. Lippard, *J. Am. Chem. Soc.* **2002**, *124*, 3993–4007.
- [35] M. Zhao, B. Helms, E. Slonkina, S. Friedle, D. Lee, J. DuBois, B. Hedman, K. O. Hodgson, J. M. J. Fréchet, S. J. Lippard, *J. Am. Chem. Soc.* **2008**, *130*, 4352–4363.
- [36] Y. Li, R. Cao, S. J. Lippard, *Org. Lett.* **2011**, *13*, 5052–5055.
- [37] J. Kuzelka, J. R. Farrell, S. J. Lippard, *Inorg. Chem.* **2003**, *42*, 8652–8662.
- [38] J. J. Kodanko, S. J. Lippard, *Inorg. Chim. Acta* **2008**, *361*, 894–900.
- [39] J. J. Kodanko, A. J. Morys, S. J. Lippard, *Org. Lett.* **2005**, *7*, 4585–4588.
- [40] J. J. Kodanko, D. Xu, D. Song, S. J. Lippard, *J. Am. Chem. Soc.* **2005**, *127*, 16004–16005.
- [41] S. Friedle, J. J. Kodanko, A. J. Morys, T. Hayashi, P. Moënnelocco, S. J. Lippard, *J. Am. Chem. Soc.* **2009**, *131*, 14508–14520.
- [42] L. H. Do, S. J. Lippard, *Inorg. Chem.* **2009**, *48*, 10708–10719.
- [43] L. H. Do, S. J. Lippard, *J. Am. Chem. Soc.* **2011**, *133*, 10568–10581.
- [44] Y. Li, J. J. Wilson, L. H. Do, U.-P. Apfel, S. J. Lippard, *Dalton Trans.* **2012**, *41*, 9272–9275.
- [45] W. A. Denny, G. W. Rewcastle, B. C. Baguley, *J. Med. Chem.* **1990**, *33*, 814–819.
- [46] J. Alonso, N. Halland, M. Nazaré, O. R'Kyek, M. Urmann, A. Lindenschmidt, *Eur. J. Org. Chem.* **2011**, 234–237.
- [47] B. Wang, M. R. Wasielewski, *J. Am. Chem. Soc.* **1997**, *119*, 12–21.
- [48] L. J. Fan, W. E. Jones Jr., *J. Am. Chem. Soc.* **2006**, *128*, 6784–6785.
- [49] E. L. Muetterties, L. J. Guggenberger, *J. Am. Chem. Soc.* **1974**, *96*, 1748–1756.
- [50] A. W. Addison, T. N. Rao, J. Reedijk, J. van Rijn, G. C. Verschoor, *J. Chem. Soc., Dalton Trans.* **1984**, 1349–1356.
- [51] T. Kurahashi, K. Oda, M. Sugimoto, T. Ogura, H. Fujii, *Inorg. Chem.* **2006**, *45*, 7709–7721.
- [52] G. M. Sheldrick, *Acta Crystallogr., Sect. A* **1990**, *46*, 467–473.
- [53] G. M. Sheldrick, *Acta Crystallogr., Sect. A* **2008**, *64*, 112–122.
- [54] P. Müller, *Cryst. Rev.* **2009**, *15*, 57–83.

Received: November 16, 2012
Published Online: February 7, 2013